

**DEVELOPMENT OF CISPLATIN DELIVERY
NANOSYSTEM WITH CHITOSAN-COATED
TITANIA NANOTUBE ARRAYS PLATFORM
TARGETING FOR NASOPHARYNGEAL
CARCINOMA**

**WAN NURAMIERA FAZNIE BT WAN EDDIS
EFFENDY**

UNIVERSITI SAINS MALAYSIA

2022

**DEVELOPMENT OF CISPLATIN DELIVERY
NANOSYSTEM WITH CHITOSAN-COATED
TITANIA NANOTUBE ARRAYS PLATFORM
TARGETING FOR NASOPHARYNGEAL
CARCINOMA**

by

**WAN NURAMIARA FAZNIE BT WAN EDDIS
EFFENDY**

**Thesis submitted in fulfilment of the requirements
for the degree of
Master of Science**

June 2022

ACKNOWLEDGEMENT

With all the praise to the Almighty that showed His Mercy, I could complete my Master dissertation in Advanced Medical and Dental Institute (AMDI), USM. Foremost, I would like to thank my supervisor, Dr Rabiatul Basria S.M.N Mydin, for her supervision, encouragement, dedication, kindness, and constant guidance throughout the study project. Next, I would express my gratitude to my co-supervisor, Prof. Ir. Dr Srimala Sreekantan (School of Materials and Mineral Resources Engineering, Engineering Campus, USM) and Dr Amirah Mohd Gazzali from the School of Pharmaceutical Science, USM for their guidance and financial assistance in completing the research project.

Besides, I am obliged to our research team, Nor Hazliana Harun, Simon I. Okekpa, Eman Salem al-Jariri and G. Ambarasan, for their generosity in spending valuable time in helping me to complete the project, especially in cell culture technique, laboratory skills, and sharing knowledge in thesis writing. Also, my colleagues were supportive and helpful friends throughout the projects. My sincere gratitude also to interns, laboratory assistants, research assistants, lecturers, and other seniors at the USM who had been involved directly or indirectly in the project. Lastly, I would like to express my deepest gratitude to my beloved parents and family members for their unwavering support, prayers, and motivation through the process of completing the research work.

TABLE OF CONTENTS

ACKNOWLEDGEMENT.....	ii
TABLE OF CONTENTS.....	iii
LIST OF TABLES.....	vii
LIST OF FIGURES.....	ix
LIST OF UNITS AND SYMBOLS.....	xx
LIST OF ABBREVIATIONS.....	xxi
LIST OF APPENDICES.....	xxiv
ABSTRAK.....	xxv
ABSTRACT... ..	xxvii
CHAPTER 1 INTRODUCTION.....	1
1.1 Introduction.....	1
1.2 Problem statement.....	3
1.3 Objective of the study.....	3
CHAPTER 2 LITERATURE REVIEW.....	4
2.1 Nasopharyngeal carcinoma.....	4
2.1.1 Chemodrug for NPC.....	6
2.1.2 Chemodrug therapy in the present, clinical and preclinical trial applications.....	11
2.2 TNA as a smart drug delivery nanosystem.....	12
2.2.1 Fabrication of TNA.....	12
2.2.2 Physiochemical properties of TNA.....	14
2.2.3 TNA potential for targeted cancer therapy.....	15
2.3 Smart drug delivery involving biopolymer coating technology.....	16

2.3.1	Type of biopolymer coating technology.....	17
2.3.2	Parameter in drug controlled released strategies.....	21
2.4	Prospects: Targeted chemodrug treatment for NPC.....	22
CHAPTER 3	METHODOLOGY.....	24
3.1	Introduction.....	24
3.2	Raw materials and chemicals.....	24
3.3	Experimental procedure.....	25
3.4	TNA nanosystem fabrication.....	27
3.4.1	Voltage effect of anodisation.....	29
3.4.2	Period of anodisation.....	29
3.5	Characterisation of TNA nanosystem for CDDP loading activity.....	30
3.5.1	Microstructure analysis via FESEM.....	30
3.5.2.	Energy dispersive X-ray analysis.....	31
3.5.3	X-ray diffraction analysis.....	31
3.6	CDDP loading strategies on TNA nanosystem.....	32
3.6.1	CDDP detection.....	33
3.6.2	CDDP loading methods.....	34
3.6.3	Determination of CDDP-TNA loading efficiency.....	34
3.7	CDDP release study strategies from chitosan-coated CDDP-TNA.....	35
3.7.1	Chitosan preparation optimisation in acetic acid solvent.....	35
3.7.2	Chitosan coating methods on CDDP-TNA.....	36
3.7.3	Chitosan coating layers optimisation.....	37
3.7.4	FTIR analysis.....	37
3.7.5	Surface properties evaluation.....	38
3.7.6	Differential pH profiles.....	38

3.7.7	Simulated body fluid profile.....	39
3.8	<i>In vitro</i> study of TNA nanosystem.....	41
3.8.1	Human cell lines model.....	41
3.8.2	Cell lines morphology analysis on TNA.....	43
3.8.3	Cytotoxicity profiles.....	43
3.8.4	<i>In vitro</i> release profiles of chitosan-coated CDDP-TNA nanosystem	44
3.8.5	Microscopy fluorescence staining analysis.....	44
CHAPTER 4	RESULTS.....	46
4.1	Introduction.....	46
4.2	Nanosystem optimisation on TNA growth.....	46
4.2.1	Observation during anodisation.....	46
4.2.2	Voltages effect of anodisation.....	49
4.2.3	Time effect of anodisation.....	50
4.3	Characterisation of chitosan-coated CDDP-TNA nanosystem.....	52
4.3.1	FESEM.....	52
4.3.2	XRD analysis.....	52
4.3.3	EDX profile.....	54
4.3.4	FTIR analysis.....	56
4.3.5	Wettability analysis.....	60
4.4	CDDP loading efficiency profiles of the TNA nanosystem.....	63
4.5	Chitosan coating and release technology.....	68
4.5.1	Concentration of acetic acid.....	69
4.5.2	Method of chitosan coating.....	72
4.5.3	Number of the chitosan coating layers.....	75

4.5.4	Release profile on different pH effect.....	84
4.5.5	The bioactivity release profile	86
4.6	Targeted CDDP release from chitosan-coated CDDP-TNA using NPC <i>in vitro</i> models.....	95
4.6.1	Cell interaction on TNA surfaces.....	95
4.6.2	Determination of IC ₅₀ for CDDP.....	95
4.6.3	Standard growth curve of NPC.....	98
4.6.4	Cytotoxicity profile.....	99
4.6.5	Intracellular profile.....	102
CHAPTER 5	DISCUSSION.....	109
5.1	TNA nanosystem characterisations for CDPP loading and targeted delivery application... ..	109
5.2	CDDP release strategies from the chitosan-coated CDDP-TNA... ..	109
5.2.1	Optimisation of chitosan coating technology.....	113
5.2.2	Physical and biochemical studies.....	115
5.3	Efficiency of targeted CDDP delivery from chitosan-coated CDDP-TNA	118
CHAPTER 6	CONCLUSION AND FURTHER PROSPECTS.....	120
6.1	Conclusion.....	120
6.2	Further prospects... ..	120
	REFERENCE	123
	APPENDICES	

LIST OF TABLES

		Page
Table 2.1	Present, clinical and preclinical works involving chemodrugs against NPC were tabulated and displayed below. Treatments, target sites and outcomes of the treatment outcomes reported in the last 20 years are presented.....	8
Table 2.2	Parameters importance in the preparation of chitosan for biopolymer coating. The parameters are vital for the biocompatibility and functionality of chitosan in biomedical applications	19
Table 3.1	General information of raw materials, chemicals, and their functions	25
Table 3.2	List of the salts used for SBF preparation. The solutions were prepared separately in a plastic container before being slowly mixed to produce SBF buffer as adapted from Kokubo & Takadama (2006)	41
Table 4.1	Element weight percentage (%) of the different properties of the TNA nanosystem at 2 K \times to observe a wider surface (with approximately 75 \times 75 μ m) for each sample. The elements detected were used to determine CDDP and chitosan on the TNA surface pre-and post-release activity. The presence of 0.19 wt.% 0.19 Pt indicated that CDDP had	

	been successfully loaded onto the TNA nanosystem.....	55
Table 4.2	FTIR peak assignments for TNA nanosystem. The major peaks for CDDP and chitosan are hydroxyl, amide I, and amine.....	57
Table 4.3	Weight difference shown by TNA before and after CDDP loading. After five cycles of CDDP loading, the weight of the TNA nanosystem increased by only 2.81 ± 1.09 %, which was not significant at $p > 0.05$. The data were collected in two independent experiments.....	64
Table 4.4	Weight difference shown by TNA before and after CDDP loading. After five cycles of CDDP loading, the weight of the TNA nanosystem increased by only 2.81 ± 1.09 %, which was not significant at $p > 0.05$. The data were collected in two independent experiments.....	67

LIST OF FIGURES

	Page
Figure 2.1	
The primary causes of NPC, available treatment and challenges for NPC therapy as adapted from Chattopadhyay <i>et al.</i> , 2017. Most researchers have claimed that EBV, lifestyle and genetics are the main contributors to NPC worldwide.....	5
Figure 2.2	
The interaction of TNP and CDDP on DNA damage was depicted schematically. TNP's negative charge at low pH (Martinho <i>et al.</i> , 2019) indicates that it could be used as a carrier for CDDP's with acidic properties (no net charge) (Kaneko, 2019) to enter the DNA sequence. When CDDP interacts with double-stranded DNA, it forms a DNA adduct, thus leading to cell death. The image was adapted from Effendy <i>et al.</i> , 2022...	10
Figure 2.3	
The biocompatibility of the NPC cells in terms of cell interaction with the TNA surfaces (average diameter of 60 nm). The elongation of filopodia demonstrated the ability of the surface to promote cell adhesion and proliferation after 48-h incubation.....	14
Figure 2.4	
Mechanical, chemical and biological properties were befitting the biomedical properties of TNA. The most frequently mentioned characteristics of TNA in the biomedical application were compiled, focusing on the cell interaction, strength and stability of the nanostructures.....	16

Figure 2.5	The research on cancer treatment in the past, existing, and future has been simplified according to Kim & Khang, 2020. Cancer location was the aim of past treatment; meanwhile, existing cancer therapy focused on the microenvironment of carcinoma. Future research on the utilisation of nanomedicine technology might be applied in drug distributions by manipulating nanosized materials.....	23
Figure 2.6	HDR-ISBT treatment in a patient with stage T3 NPC. Image (a) illustrated the brachytherapy application via an inserted needle adapted from Murakami <i>et al.</i> , 2020, (b) displayed the 2D image of brachytherapy prototype and (c) showed the example of patient with the device.....	23
Figure 3.1	Experimental workflow for targeted CDDP delivery nanosystem with TNA.....	26
Figure 3.2	Setup of TNA anodisation in organic electrolyte. The distance between the cathode (Ti) and platinum (Pt) foil (anode) was maintained at 2 cm throughout the process	27
Figure 3.3	Annealing profile of TNA in argon gas. The soaking time of the TNA nanosystem was set for 2-h at 400 °C with heating and cooling of 5 °C per minute	28
Figure 3.4	Flowchart of CDDP detection. An illustrative graphic of CDDP detection was adapted from Fisher <i>et al.</i> , 2016. The CDDP concentration was determined in the order of CDDP, OPDA, phosphate buffer pH 6.8, and DMF with ratio (1:1:2:6).....	33

Figure 3.5	The outcome of the CDDP loading and chitosan coating processes. Image (a) showed the process of vacuum drying method of CDDP-TNA, (b) drying method of chitosan coating by dipping and spin-coating, (c) the outcome of (b) after 90 mins drying, and (d) the end-result of CDDP-TNA surface drying sample. Accumulation of dried chitosan observed for image (c).....	36
Figure 3.6	Sink condition of TNA nanosystem samples in SBF buffer described in ISO 23317/2007. The analysis was performed in two technical replicates, with three reading for each sample was taken.....	40
Figure 4.1	Anodisation bubbles produced by the fabrication of TNA. At the early stage of anodisation, a small amount of bubble released was observed (a). Image (b) showed the observation at the later stage of anodisation.....	47
Figure 4.2	Anodisation profile of the TNA nanosystem. Current density over time curve displaying the anodisation phases of the TNA nanosystem. (a) Initial oxidation of Ti to TNA, (b) pits formation and enlargement of the oxide layer, and (c) continuous growth of TNA until 60 mins. The anodisation curve represents one sample, as all samples showed a similar trend during TNA nanosystem anodisation.....	48
Figure 4.3	Current density and FESEM view of TNA nanosystem anodised at 30 V and 60 V for 30 mins. The nanostructure of TNA of 30	

	V showed the best morphology of individual nanotubes; meanwhile, protrusion of TNA was observed at 60 V.....	50
Figure 4.4	Side view of the TNA nanosystem anodised at 30 mins and 60 mins. The length of the TNA nanosystem (n = 4) anodised for 30 mins was 277.63 ± 14.67 nm, whereas the TNA nanosystem anodised for 60 mins was 832.10 ± 34.17 nm, which demonstrated a statistically significant difference at $p < 0.000...$	51
Figure 4.5	XRD analysis of Ti, the un-annealed TNA nanosystem, and the annealed TNA system. The formation of new peaks is labelled with a red arrow to indicate the changes in the crystallinity phase. The Ti peak represented the substrate, whereas the anatase (A) represented the TNA nanosystem's crystallinity shape.....	53
Figure 4.6	FTIR analysis of TNA, CDDP-TNA, and chitosan-coated CDDP-TNA. The peaks at 2176 and 595 cm^{-1} indicated the Ti–O–Ti stretching band peaks of TNA. The presence of CDDP was identified based on the peak in the FTIR spectrum at 1671 cm^{-1}	58
Figure 4.7	FTIR spectrum of the post-release chitosan-coated CDDP-TNA collected over the range of $4000\text{--}500\text{ cm}^{-1}$ at three different positions; a, b, and c. Peaks at 2163 cm^{-1} were ascribed to the TNA nanosystem and were the same as those in the spectrum of the TNA nanosystem. The C–H band ($3280\text{--}3357\text{ cm}^{-1}$) suggested that chitosan remained. The peaks at 1641 cm^{-1} were	

	previously identified as N–H bands from CDDP loaded onto the TNA.....	59
Figure 4.8	Wettability analysis of the TNA nanosystem. The highest contact angle recorded for the chitosan-coated CDDP-TNA was due to the hydrophilic properties of the compounds. Data were expressed as mean \pm SD (n = 5). The significant difference between samples was expressed with an asterisk to indicate the significance of the pair (p < 0.05).....	61
Figure 4.9	Wettability analysis of the studied sample. The water contact angle of each sample was examined by using a goniometer and visualised by using ImageJ software. The angle of wettability was displayed as mean \pm SD (n = 5).....	62
Figure 4.10	Histogram displaying the loading efficiency of the TNA nanosystem under various CDDP loading conditions. Vacuum drying showed a more significant difference (***) than the nonvacuum sample, whereas the top-filling method displayed higher efficiency (***) than the overnight immersion. Compared with the TNA nanosystem anodised for 30 mins at 300 nm, the TNA nanosystem anodised for 60 mins at 800 nm demonstrated longer lengths and higher CDDP encapsulation efficiency. p < 0.05 (*) and p < 0.01 (**), n = 3.....	65
Figure 4.11	CDDP detection standard curve at 706 nm. Data are expressed as means \pm SD from the lowest (0.125 mM) to the highest (1.0 mM) concentration of CDDP. The data are presented as means	

	± SD from three independent tests with four technical replicates.....	66
Figure 4.12	Differences in loading efficiency between TNA nanosystem with two different lengths. Significant differences between these two groups were determined with $p = 0.001$, $n = 3$	68
Figure 4.13	Biphasic release study of CDDP-TNA, chitosan-coated CDDP-TNA (1 % v/v) and chitosan-coated CDDP-TNA (2 % v/v). (a) Burst release and (b) prolonged release profiles. Comparison with CDDP-TNA revealed no significant difference in the release profile of both 1 % (v/v) and 2 % (v/v) chitosan-coated CDDP-TNA ($p > 0.05$).....	70
Figure 4.14	Cytotoxicity study on chitosan-coated CDDP-TNA (1 % v/v) and chitosan-coated CDDP-TNA (2 % v/v) through comparison with untreated cells and TNA only. A significant difference was noted between cells treated with chitosan-coated CDDP-TNA (2 % v/v) and untreated cells, $p = 0.046$, $n = 4$	71
Figure 4.15	FESEM analysis of chitosan-coated TNA nanosystems. (a) bare TNA nanosystem, (b) 0.5 % (w/v) chitosan-coated TNA (c) 1.0 % (w/v) chitosan-coated TNA and (d) 2.0 % (w/v) chitosan-coated TNA. The degree of chitosan coverage varied depending on the concentration of chitosan used: (b) showed a vague appearance of TNA nanosystems, whereas (c) and (d) showed entire coverage with no appearance of TNA nanosystems.....	72

Figure 4.16	The burst CDDP release profile from different chitosan coating techniques on CDDP-TNA. A significant release pattern was observed between CDDP-TNA and the chitosan-coated CDDP-TNA (top-filled) with $p = 0.001$ from four replicate experiments. The data are presented as means \pm SD and analysed with Student's t-test, with $p < 0.05$ considered statistically significant.....	74
Figure 4.17	Cumulative CDPP release profile from CDDP-TNA with different polymer coating layers. There are no significant differences observed in the release profile of CDDP from all coating layers. The data from triplicate experiments are presented as means \pm SD and analysed with Student's t-test.....	76
Figure 4.18	Evaluation of the toxicity of the chitosan-coated TNA nanosystem against Kasumi-1 cells. The tested systems, except for the TNA nanosystem (48-h) coated with five layers of chitosan and the TNA nanosystem (72-h) coated with three layers of chitosan, exerted no significant inhibitory effect.....	78
Figure 4.19	Evaluation of the cytotoxicity of chitosan-coated TNA nanosystems against HEK 293 cells. The viability of the cells decreased to less than 80 % upon interaction with the chitosan-coated TNA nanosystem.....	80
Figure 4.20	Cytotoxicity of chitosan-coated TNA nanosystem against NPC cells; a) NPC/HK-1 and b) C666-1. The coating layer exhibited an inhibitory effect as the number of layers and incubation periods were increased. All adherent-type cells treated with the	

	TNA nanosystem coated with three and five layers of chitosan exhibited significant inhibition ($p < 0.05$).....	83
Figure 4.21	Cumulative CDDP release from chitosan-coated CDDP TNA. The biphasic phase of burst- (a) and prolonged-release (b) phase was observed at different pH levels. The data are presented as means \pm SD and analysed with Student's t-test, with $p < 0.05$ considered statistically significant.....	85
Figure 4.22	FESEM and EDX profiles of chitosan-coated CDDP TNA in the burst-release phase. (a) CDDP-TNA, (b) chitosan-coated TNA nanosystem and (c) chitosan-coated CDDP-TNA. The non-detection of Pt suggested a fully covered CDDP-TNA surface.....	87
Figure 4.23	FESEM and EDX profiles of chitosan-coated CDDP TNA after CDDP release activity. (a) CDDP-TNA, (b) chitosan-coated TNA nanosystem and (c) chitosan-coated CDDP-TNA. The non-detection of Pt was probably caused by the complete release of the CDDP, as noted in the optimisation studies	87
Figure 4.24	Ion content analysis using ICP-OES on CDDP release at d-2 and d-10 from chitosan-coated CDDP TNA. The Na ions were observed and presented as means \pm SD after normalised with blank (SBF buffer) and analysed with Student's t-test, with $*p < 0.05$ considered statistically significant, while $****p < 0.000$ (extremely significant).....	90
Figure 4.25	Ion content analysis using ICP-OES on CDDP release at d-2 and d-10 from chitosan-coated CDDP TNA. The P ions	

observed indicated apatite formation. The data are presented as means \pm SD after normalised with blank (SBF buffer) and analysed with Student's t-test, with *p < 0.05 considered statistically significant, while ****p < 0.000 (extremely significant) 91

Figure 4.26 Ion content analysis using ICP-OES on CDDP release at 2 and 10 days from chitosan-coated CDDP TNA. Ca contents decreased in the TNA nanosystem without chitosan but increased in the chitosan-coated TNA nanosystem and chitosan-coated CDDP-TNA. The data are presented as means \pm SD after normalised with blank (SBF buffer) and analysed with Student's t-test, with *p < 0.05 considered statistically significant, while ****p < 0.000 (extremely significant) 93

Figure 4.27 Ion content analysis using ICP-OES on CDDP release at 2 and 10 days from chitosan-coated CDDP TNA. Pt contents in the CDDP-TNA systems were the highest, thus required 10-fold dilutions. The presence of Pt indicated the successful release of CDDP after loading onto the TNA nanosystem surface. The data are presented as means \pm SD after normalised with blank (SBF buffer) and analysed with Student's t-test, with *p < 0.05 considered statistically significant, while ****p < 0.000 (extremely significant) 94

Figure 4.28 FESEM images of NPC and HEK 293 cells on TNA surfaces after 48-h of incubation. (a–c) FESEM observation under low magnification and wide view and (b) under high magnification.

	The presence of the TNA nanosystem (yellow arrows) and the elongation of cell filopodia (red arrows) were highlighted, supporting the biocompatibility of the TNA nanosystem for cell attachment. (a) and (b) HEK 293, (c) and (d) C666-1 and (e) and (f) NPC/HK-1 cells.....	96
Figure 4.29	Cytotoxicity of CDDP against the studied cells. IC ₅₀ was calculated and determined from the graph. IC ₅₀ of NPC/HK-1 was 0.5 mM, whereas that of C666-1 recorded at 0.05 mM CDDP. This value was then applied in the study on CDDP-TNA release profiles.....	97
Figure 4.30	Mean ± SD of NPC cells (NPC/HK-1 and C666-1) cultured in complete media for d-7 with initial seeding density (1×10^4), n = 4. The highest NPC/HK-1 was achieved at 4×10^4 (d-3), while C666-1 showed a peak number at 3.7×10^4 (d-5)	98
Figure 4.31	Cytotoxicity investigation involving NPC/HK-1 cell lines treated for 24-, 48- and 72-h with CDPP, chitosan, CDDP-TNA and chitosan-coated CDDP-TNA. Inhibitory effects on the samples were explored. Cell inhibition at 48-h was more significant than untreated cells after cells interact with the CDDP-TNA and chitosan-coated CDDP-TNA.....	99
Figure 4.32	Cytotoxicity of C666-1 cell lines treated for 24-, 48- and 72-h. Cells treated with CDDP-TNA were inhibited by more than 40 % after 72-h of treatment, while chitosan-coated CDDP-TNA treatment showed inhibition exceeding 80 %.....	101

Figure 4.33	Intracellular activities of HK-1 cells against the TNA nanosystem. Cell damage was determined based on the shrinkage of cells, the number of cells and the presence of cell fragments. The cells exposed to CDDP-TNA with or without chitosan coating appeared to be severely affected, given that almost no viable cells remained as indicated by the expression of the staining colours.....	106
Figure 4.34	Intracellular activities of C666-11 cells against the TNA nanosystem. Cell damage upon treatment with CDDP-TNA in the absence or presence of chitosan was seen with the expression of red and orange-green colour cells. Analysis with an inverted light microscope showed a small number of cells. This result indicated the destruction of the cancer cell.....	108
Figure 5.1	Illustrative description of the present work. The image depicts the workflow in detail from the anodisation of TNA, CDDP loading, optimisation of chitosan coating, CDDP release profile to the cytotoxicity evaluation of CDDP-TNA.....	112

LIST OF UNITS AND SYMBOLS

cm	centimetre
°	degree
°C	degree celsius
G	gram
K	kilo
L	litre
μ	micro
mA	milliampere
mL	millilitre
mm	millimetre
mΩ	milliohm
mg	milligram
M	molar
nm	nanometre
%	percentage
rpm	revolutions per minute
V	voltage
v/v	volume per volume
wt. %	weight percentage

LIST OF ABBREVIATIONS

Ca	calcium
CaCl ₂	calcium chloride
CDDP-TNA	cisplatin-loaded onto TNA
CO ₂	carbon dioxide
Cu	copper
D	day (s)
DMEM	Dulbecco's modified eagle media
DMF	N, N-Dimethylformamide
DMSO	dimethyl sulfoxide
EA	electrochemical anodisation
EBV	Epstein-Barr virus
EDX	energy dispersive X-ray
FBS	foetal bovine serum
FESEM	field emission scanning electron microscope
FTIR	Fourier transform infrared spectroscopy
h	hour/s
HCl	hydrogen chloride
HEPES	4-(2-hydroxyethyl)-1-piperazineethanesulfonic acid
HSE	Health Safety Executive
IC ₅₀	half maximal inhibitory effect
ICP-OES	ion-coupled plasma optical emission spectroscopy
K ₂ HPO ₄ ·3H ₂ O	potassium hydrogen phosphate trihydrate
KCl	potassium chloride

MCA	Medicines Control Agency
min (s)	minutes
MgCl ₂ .6H ₂ O	magnesium chloride hexahydrate
MTS	3-(4,5-dimethylthiazol-2-yl)-5-(3-carboxymethoxyphenyl)-2-(4-sulfophenyl)-2H-tetrazolium (MTS); CellTiter96 Aqueous One Solution MTS reagent powder
Na	sodium
Na ₂ SO ₄	sodium sulphate
NaCl	sodium chloride
NaHCO ₃	sodium bicarbonate
NH ₄ F	ammonium fluoride
NPC	nasopharyngeal carcinoma
OPDA	o-Phenylenediamine
P	phosphorus
Pt	platinum
PBS	phosphate buffer saline
pH	potential of hydrogen
RPMI 1640	Roswell Park Memorial Institute
RT	room temperature
s	second (s)
SBF	simulated body fluid
SD	standard deviation
Ti	titanium foil
TNA	titania nanotube arrays
Tris base	tris(hydroxymethyl)aminomethane

USA	United State of America
XRD	x-ray diffraction analysis

LIST OF APPENDICES

Appendix A	Standard curve of ion for ICP-OES
Appendix B	List of publications and conferences
Appendix C	Academic award and intellectual property

**PEMBANGUNAN NANOSISTEM PENYAMPAIAN CISPLATIN DENGAN
PLATFORM TATASUSUNAN TIUBNANO TITANIA BERLAPIK KITOSAN
MENSASARKAN KARSINOMA NASOFARING**

ABSTRAK

Rawatan ubat kemo yang ada untuk karsinoma nasofaring tahap lanjut (NPC) melalui cisplatin (CDDP) mempunyai beberapa batasan seperti ketoksikan pembatasan dos, biodistribusi tidak spesifik, kemunculan sel barah kebal dan pelbagai kesan sampingan. Pelepasan penyampaian CDDP yang disasarkan dan terkawal menggunakan nanosistem pintar nanotiub titania tersusun (TNA) mungkin menawarkan pendekatan baru untuk memperbaiki batasan tersebut. Dalam kajian ini, TNA difabrikasi, dicirikan dan dioptimumkan oleh anodisasi elektrokimia untuk pemuatan CDDP. Kecekapan pemuatan TNA yang dimuat CDDP (CDDP-TNA) dikaji menggunakan dua kaedah: kaedah pengisian bahagian atas dan perendaman. Pencirian dilakukan dengan menggunakan mikroskop elektron pengimbasan pancaran medan, penyebaran tenaga sinar-X, pembelauan sinar-X, spektrometer pancaran optik-plasma gandingan aruhan (ICP-OES), spektroskopi inframerah transformasi Fourier, spektrofotometri dan ujian kebasahan. CDDP-TNA yang bersalut kitosan biopolimer dioptimumkan dari segi kepekatan asid asetik untuk penyediaan 10 mg/mL kitosan, kaedah salutan, bilangan lapisan salutan, dan keserasian-bio lapisan salutan kitosan. Kegiatan pelepasan CDDP dari CDDP-TNA yang bersalut kitosan selanjutnya disiasat dalam pelbagai sistem perendaman larutan penimbal fosfat dengan nilai pH yang berbeza, simulasi cecair badan dan sistem *in vitro* NPC yang disasarkan. Pemerhatian intraselular lebih lanjut dilakukan dengan menggunakan mikroskop pendarfluor. Dapatan menunjukkan bahawa CDDP dimuat secara efisien ke nanosistem TNA dengan kaedah pengisian bahagian atas, dengan profil kecekapan pemuatan 98.95 ± 7.02 % dan disahkan oleh ICP-OES dengan pengesanan ion platinum

(Pt). Satu lapisan CDDP-TNA yang bersalut kitosan dan terisi bahagian atas yang diformulasikan dalam 1 % (v/v) asid asetik menghasilkan pelepasan CDDP yang optimum dengan sifat salutan bioserasi hingga 10 hari masa kajian. Tingkah laku pelepasan CDDP jangka panjang dari nanosistem ini juga dicapai dalam pelbagai sistem model terangsang. Selanjutnya, kecekapan fungsian CDDP-TNA yang bersalut kitosan ditunjukkan menggunakan penyampaian yang disasarkan ke arah model garis sel NPC, di mana 50 % sel NPC dihambat setelah pendedahan 48 jam. Dalam aplikasi terapi barah yang disasarkan pada masa depan, penyelidikan menyeluruh mengenai pengawalan lapisan salutan kitosan diperlukan untuk peningkatan dalam aktiviti pelepasan terkawal CDDP dari nanosistem ini.

**DEVELOPMENT OF CISPLATIN DELIVERY NANOSYSTEM WITH
CHITOSAN-COATED TITANIA NANOTUBE ARRAYS PLATFORM
TARGETING FOR NASOPHARYNGEAL CARCINOMA**

ABSTRACT

Present chemodrug treatment for advanced-stage nasopharyngeal carcinoma (NPC) via cisplatin (CDDP) have limitations such as non-specific biodistribution, dose-limiting toxicities, the emergence of resistant cancer cells and various side effects. Targeted and controlled release of CDDP delivery using titania nanotube arrays (TNA) smart nanosystem may offer a new approach to improve those limitations. TNA was fabricated, characterised, and optimised by electrochemical anodisation for CDDP loading in this study. The CDDP-loaded TNA (CDDP-TNA) encapsulation efficiency was studied using two methods: top-filling and immersion methods. The characterisation was performed using field emission scanning electron microscopy, energy dispersive X-ray, X-ray diffraction, ion-coupled plasma–optical emission spectrometry, Fourier transform infrared spectroscopy, spectrophotometry and wettability test. Biopolymer chitosan-coated CDDP-TNAs were optimised in terms of concentrations of acetic acid for 10 mg/mL chitosan preparation, coating methods, number of coating layers, and biocompatibility of chitosan coating layers. The CDDP release activities from chitosan-coated CDDP-TNA were further investigated in various phosphate buffer saline immersion systems with different pH values, simulated body fluid, and targeted NPC *in vitro* system. Further intracellular observation was performed using fluorescence microscopy. Findings indicated that CDDP was efficiently loaded onto a TNA nanosystem by top-filling method, with an encapsulation efficiency profile of 98.95 ± 7.02 % and confirmed by ICP–OES with detection of platinum (Pt) ions. A layer of top-filling chitosan-coated CDDP-TNA

formulated in 1 % (v/v) acetic acid yielded the optimum CDDP release with biocompatible coating properties up to ten days study period. The nanosystem's long-term sustained CDDP release behaviour was also achieved in various stimulated model systems. Furthermore, the functional efficiency of chitosan-coated CDDP-TNA was shown using targeted delivery towards the NPC cell line model, where 50 % of NPC cells were inhibited after 48-h exposure. In future targeted cancer therapy applications, a comprehensive investigation on controlling chitosan coating layers is needed to enhance the controlled release activities of CDDP from the nanosystem.

CHAPTER 1

INTRODUCTION

1.1 Introduction

Nasopharyngeal carcinoma (NPC) has been one of Malaysia's most often reported cancers over the past five years, based on Globocan (2020) data. An unhealthy lifestyle, Epstein Barr virus (EBV), and inherited characteristics had been associated with NPC. NPC's treatment is challenging, mainly caused by the location of tumours inflexible for surgical removal. Although chemoradiation, the current treatment for NPC, has shown to be effective, various adverse effects have been reported, including anaemia, diarrhoea, nausea, and, at worst, kidney failure. Various strategies for NPC-targeted drug administration, including smart, targeted drug delivery systems, extensive researches have been conducted to address the limitations mentioned earlier and to increase treatment efficiency and reduces mortality.

The chemotherapeutic cisplatin (CDDP) was chosen as the study treatment because of its capacity to break down double-stranded DNA, preventing cancer cells from replicating and therefore inhibiting cell growth. Smart chemodrug delivery systems have been integrated into cancer therapy and thoroughly investigated to alleviate the drawbacks of conventional treatment, such as non-specific targets that harm healthy cells. Nanomaterials, particularly titania nanotube arrays (TNA), are widely employed due to their unique properties, even presented with small dimensions and large surface area per volume. By combining CDDP with TNA as a nanocarrier, the chemodrug could be delivered to a specified location without damaging other cells, overcoming the limitations of single treatment. CDDP was loaded onto TNA with a chitosan coating for controlled release in this study.

The present study demonstrated the optimal morphological parameters and CDDP loading onto a TNA nanosystem (CDDP–TNA) method with maximum encapsulation efficiency. TNA nanosystem demonstrated various properties that are fitted for biomedical implant development. These properties include the capability to promote cell adhesion, differentiation and replication. The one-end nanotube design of the nanosystem promoted efficient and facile drug entrapment either via a direct method or incorporation during TNA fabrication. The biopolymer coating has antibacterial features, good biocompatibility and biodegradability help develops the smart chemodrug delivery nanosystems. Although the application of chitosan as a coating layer for drug-loaded TNA was explored before, the optimal conditions of the nanosystem are still unclear.

The most commonly studied parameters on controlling the rate of drug release are the concentration of diluent used, the method of chitosan coating and the number of chitosan coating layers. The pH of immersion buffers was found to influence the drug release activities, which is believed to be caused by its effect on the chitosan degradation rate. The pH of the environment wherein the drug will be released is critical as the pH of the targeted organ may be different from the normal pH. In addition, multiple release systems, such as PBS, SBF, and *in vitro* culture conditions that mimic physiological fluids were performed to comprehensively understand the chitosan-coated CDDP–TNA's behaviour. The CDDP release was quantified through spectrophotometry. The nanosystem's pre-and post-release characterisations were performed to further confirm CDDP loading and release activity. The surface characteristics, encapsulation efficiency, release profile and *in vitro* controlled CDDP release of the chitosan-coated CDDP–TNA nanosystem was fully covered in this work.

1.2 Problem statement

An efficient therapeutic loading and release technique from an NPC-targeting chitosan-coated CDDP-TNA system is essential for establishing smart chemodrug delivery systems.

1.3 Objective of the study

General objective

To develop an efficient, targeted chemodrug delivery nanosystem using chitosan-coated CDDP-TNA on NPC cell line models.

Specific objectives

- a) To fabricate by using electrochemical anodisation and characterise the TNA nanosystem for CDDP delivery with FESEM, EDX and XRD profiles.
- b) To optimise CDDP loading and release from the TNA nanosystem with chitosan coating strategies by spectrophotometry measurement.
- c) To study the bioactivity profile of chitosan-coated CDDP-TNA in simulated body fluid using ion-coupled plasma optical emission spectroscopy.
- d) To investigate the functional efficiency of CDDP targeted delivery using chitosan-coated CDDP-TNA on NPC cell line models by using a cell proliferation kit.

CHAPTER 2

LITERATURE REVIEW

2.1 Nasopharyngeal carcinoma

NPC is a malignant epithelial cancer cell found in the head and neck areas (The Johns Hopkins University, 2021). Cancer cells originating from the nasopharynx are described as squamous cells and act differently from other neck and head cancer cells and are highly associated with the Epstein–Barr virus (EBV). The three diagnostic subtypes of NPC include type 1, involving keratinising squamous cancer cells that are closely related to EBV was reported in 70 – 80 % of NPC cases; type 2, which comprises differentiated non-keratinising carcinoma and type 3, which is the most common type of NPC and includes undifferentiated non-keratinising cancer cells (Sinha & Gajra, 2020; Chattopadhyay *et al.*, 2017).

The NPC cases reported in the east and southeast Asia (mainly southern China) are caused by community dietary habits, which involve consuming salted and fermented dishes (Kang *et al.*, 2020; Jia *et al.*, 2010). Moreover, unhealthy lifestyle habits, such as tobacco smoking, high alcohol consumption and unhealthy diet, contribute to the high incidence of NPC (Okekpa *et al.*, 2019; Chang & Adami, 2006). In agreement with Yeo *et al.*, 2018 and data from the Ministry of Health Malaysia (2016), ethnicity, family history, and genetics are other factors of NPC occurrence in Malaysia. The native migration and cultural exchange between native Southern Chinese with other races and ethnicities led to a significant dispersed distribution of NPC cases (Simons, 2011). The general concept of factors, treatment and challenges of current treatment for NPC is summarised in Figure 2.1.

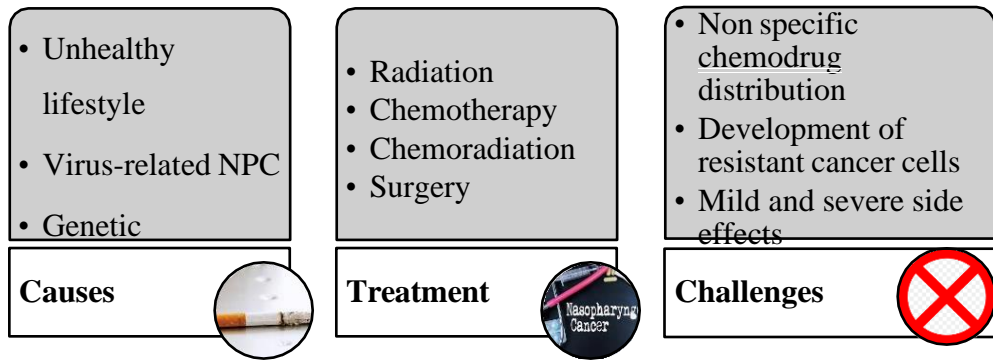


Figure 2.1 The primary causes of NPC, available treatment and challenges for NPC therapy as adapted from Chattopadhyay *et al.*, 2017. Most researchers have claimed that EBV, lifestyle and genetics are the main contributors to NPC worldwide.

In Malaysia, NPC was often evident in the Chinese population as a whole and the Bidayuh community for the Borneo population (Linton *et al.*, 2021; Abdullah *et al.*, 2019; Yeo *et al.*, 2018). According to Abdullah *et al.* (2019), one of the factors contributing to NPC data in Malaysia’s Chinese population may be attributed to community dispersion in the city region, allowing Chinese people to be more likely to receive NPC treatment than other people, thus resulting in a higher record of data compared to other ethnic. On the other hand, Linton *et al.* (2021) and Yeo *et al.* (2018) centred their NPC data on genetic susceptibility that was similar to the genetic profile of Chinese in Indochina or South China, notably Bai-Yue people. The age-standardised rate (ASR) for NPC in Bidayuh is also equivalent to the highest ASR globally, implying that the genetic link between NPC and NPC is the most likely contributing factor. Due to a hereditary tendency that has been passed down through generations, males are more prone to NPC than females. Even though there are many different perspectives on the causes of NPC, the three main factors depicted in Figure 2.1 have remained the most important factors, allowing future researchers to concentrate their efforts on effective treatments such as chemodrugs, radiation, or conventional surgery.

2.1.1 Chemodrug for NPC

The capabilities of cancer cells to replicate and be modified at an abnormal rate are the common issues that cause difficulties in treatment. Although conventional treatment does have a high rate of success in the past, the treatment's drawbacks have also been reported, including drug insolubility and non-specific target treatment, thus causing damage to the surrounding cells (Wang *et al.*, 2017; Wen *et al.*, 2015). As a result, chemodrug failure was noted either resulted in chemotherapy resistance, the high risk for post-treatment infection or drug toxicity (Zugazagoitia *et al.*, 2016). Chemotherapy and radiotherapy treatments are performed to eliminate cancer effectively (National Cancer Institute, 2020). However, noticeable side effects, such as nausea, lack of appetite and hair loss, have been associated with these treatment strategies. The outcomes of standard treatments become a hindrance and concern to patients and thus lead to the failure to continue treatment.

As tabulated in Table 2.1, many studies have been conducted to improve cancer therapy with combinations of chemodrugs. The effectiveness of cancer therapy technology has evolved by introducing chemodrug combinations, such as cisplatin (CDDP) and doxorubicin, CDDP and paclitaxel and CDDP and gemcitabine (Dasari & Tchounwou, 2014). The applications of multidrug treatment had developed multidrug resistance, which is responsible for the increasing number of deaths of cancer patients (Bukowski *et al.*, 2020), leading to new progress of NPC treatment towards chemoradiation as tabulated in Table 2.1 due to limitations above. The frequent administration of treatment and recurrent cancer are the main reasons for drug resistance caused by higher chemodrugs doses of chemotherapy. Additional works have been performed to overcome the stated problems while improving the effectiveness of the provided treatments.

CDDP, chemically recognised as *cis*-diamminedichloroplatinum (II) based on its chemical structure as presented in Figure 3.4, is a widely used chemodrug for cancer treatment (Dasari & Tchounwou, 2014). Dasari & Tchounwou, 2014, reported that the use of CDDP for carcinoma had achieved its limits given that a single treatment with CDDP is ineffective. Aldossary, 2019, reported that the mechanism of action of CDDP is associated with the potential of CDDP to cross-link with the uracil bases on DNA to produce DNA adducts that cause DNA damage and induce cancer cell death by blocking DNA repair. Even though CDDP is a powerful chemodrug for NPC treatment, it also presented limitations such as high carcinogenicity and sensitivity to light which is tricky for targeted chemodrug delivery technology. The present work was performed to maximise CDDP loading and maintain the effectiveness of CDDP against NPC cells.

Table 2.1 Present, clinical and preclinical works involving chemodrugs against NPC were tabulated and displayed below. Treatments, target sites and outcomes of the treatment outcomes reported in the last 20 years are presented.

Stage of study	Chemodrugs(s)	Target samples	Outcome
Present study (Ministry of Health Malaysia, 2016)	CDDP Fluorouracil Docetaxel Carboplatin	Human	Presented with nausea, vomiting, renal and auditory dysfunction, myelosuppression and electrolyte imbalance. Other side effects were diarrhoea, hypersensitivity and myocardial infraction.
Present study (DeNittis <i>et al.</i>, 2002)	CDDP Adjuvant CDDP/5-fluorouracil (5-Fu) radiation therapy (EBXRT) 70 Gy/7 weeks + 3 cycles of concurrent CDDP subsequently continued with adjuvant treatment for 2–3 weeks.	Human	The 3-year survival rate of 100%. No evidence of neck and related organ failure. Promoted patient survival and local-regional control.
Clinical (Peng <i>et al.</i>, 2021)	Radiotherapy followed by adjuvant chemotherapy and adjuvant chemotherapy followed by concurrent chemoradiation.	Advanced NPC of random patients.	Adjuvant chemotherapy was highly effective for distant metastasis with a high risk of treatment failure. Ineffective treatment also observed, suggesting resistance against CDDP-based cancer therapy.
Clinical study (n = 50), conceptualisation (Zhang <i>et al.</i>, 2021^a)	Concurrent chemoradiotherapy followed by adjuvant chemotherapy (Gemcitabine and CDDP or 5-Fu and CDDP)	Fifty patients with advanced NPC divided into two groups.	The expected outcome of CDDP and 5-Fu was to be slightly ineffective considering that these chemodrugs target lower distant tumours.
Clinical (Zhang <i>et al.</i>, 2019)	Gemcitabine and CDDP with and without the addition of concurrent chemoradiotherapy	Newly diagnosed stage III and IVB, n = 480	Single treatment resulted in a high incidence of anaemia, nausea, vomiting, thrombocytopenia and neutropenia.

Preclinical (Fu et al., 2021)	Lipid–polymer hybrid NPs with the addition of CDDP and afatinib (AFT).	<i>In vitro</i> (HONE1) <i>In vivo</i> (BALB/C mice)	CDDP, AFT and NPs (single treatment) demonstrated anti-cancer properties. Combination CDDP–AFT treatment resulted in higher toxicity than a single treatment, whereas AFT/CDDP loaded into lipid–polymer NPs showed higher cytotoxicity than the combination drug treatment.
Clinical (You et al., 2020)	5-Fu (5 g/m ²) administered for 120 h and CDDP (100 mg/m ²) on day one and every three weeks (6 times)	NPC patients (n = 126)	No significant gastrointestinal injury or toxicity was observed. Patients with higher stages of NPC presented xerostomia, dermatitis and mucositis. Less number of patients developed hearing loss and trismus after chemotherapy plus radiotherapy.
Preclinical (Zhang et al., 2021^b)	Dasatinib self-assembled nanoparticles (NPs) coated with hyaluronic acid (THD-NP)	<i>In vitro</i> NPC cells (HNE1) and CDDP-resistant HNE1/DDP	THD-NP had a highly toxic effect on the two cell lines. THD-NP was effective in delivering Dasatinib and showed potential for preventing multidrug resistance caused by chemodrug administration.
Preclinical (Wang et al., 2020)	Paclitaxel (Taxol) and Neferine (NEF) as tumour cell sensitisers before chemotherapeutic treatment.	<i>In vitro</i> 5-8F, CNE-1, 5-8F/Taxol, CNE-1/Taxol <i>In vivo</i> (BALB/C male nude mice)	NEF could overturn the NPC cell resistance against Taxol <i>in vitro</i> and <i>in vivo</i> . NEF also successfully increased the Taxol sensitivity of NPC cells.
Preclinical (Guo et al., 2020)	Poly(lactide-co-glycolide) copper oxide NPs coated with either doxorubicin or docetaxel with folate conjugate.	<i>In vitro</i> (HNE-1)	Reduction in cells with minimal copper oxide cytotoxicity.

As shown in Table 2.1, the CDDP has always been the best strategy for treating NPC either as a single or combined treatment. The interaction of the positive charge titanium dioxide (TiO_2) NP and the no charge CDDP can be presumed to constitute the mechanism of action of CDDP with (TiO_2) in NP form, as shown in Figure 2.2. The surface charge of TiO_2 can carry the CDDP, but the adsorption may be weaker, resulting in CDDP loss before it reaches the desired site. The internalisation, cytotoxicity, and chemodrug resistance induced by CDDP during contact with the plasma membrane, according to Martinho *et al.* (2019). The introduction of CDDP caused changes in membrane permeability and integrity. As stated in 2.1.1, combining one chemodrug with another may result in the development of resistance cancer; therefore, focusing on using one chemodrug with an efficient nanocarrier may result in a better outcome, particularly if the nanocarrier has good biocompatibility with the cancer environment.

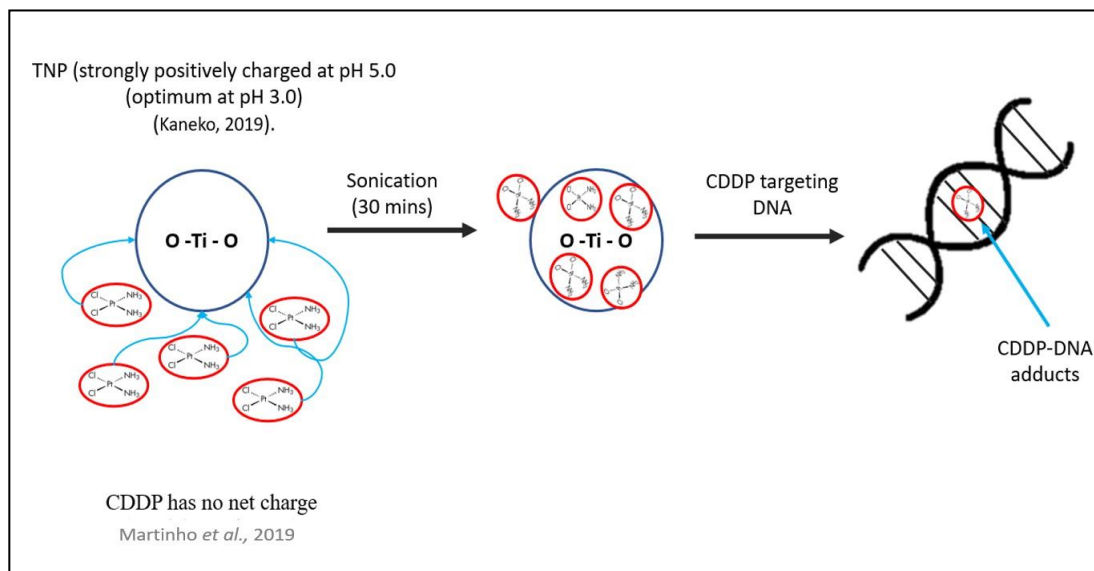


Figure 2.2 The interaction of TNP and CDDP on DNA damage was depicted schematically. TNP's negative charge at low pH (Martinho *et al.*, 2019) indicates that it could be used as a carrier for CDDP's with acidic properties (no net charge) (Kaneko, 2019) to enter the DNA sequence. When CDDP interacts with double-stranded DNA, it forms a DNA adduct, thus leading to cell death. The image was adapted from Effendy *et al.*, 2022.

2.1.2 Chemodrug therapy in the present, clinical and preclinical trial applications.

Localised and targeted therapies have been introduced to overcome the limitations of conventional cancer treatment. Targeted therapy, which aims to increase the effectiveness of chemodrug treatment at the level of proteins or genes highly associated with cancer development while avoiding non-specific drug binding, has been introduced (Vasir & Labhasetwar, 2005^a). Immunoscintigraphy (radioisotope-conjugated targeted antibodies) for imaging is an example of available targeted cancer treatment (Padma, 2015). Localised cancer therapy usually involves the latest technology, such as nanotechnology. Drugs are delivered through passive diffusion by targeting overexpressed tumour markers, permeable cancer cells or an environment that stimulates drug release from nanocarriers to the target site (Wolinsky *et al.*, 2012).

As displayed in Table 2.1, liposome vesicles, polymer micelles, dendritic polymers and various nanostructures are commonly used in localised cancer therapy. Size, stability and large surface area are the best features that guarantee the high success rate of nanocarriers (Lombardo *et al.*, 2019; Wang *et al.*, 2017). Nanoparticles (NP) have been studied as drug carriers due to their small physical size, stability, large surface area and capability to enter the cell membrane to cause cell damage (Song *et al.*, 1997). NPs act as a double-edged sword given their size advantages and limitations due to their possibility for aggregation, leading to toxicity. The interactions of cancer cells and NPs via endocytosis cause dysfunction in the regular activity of cells (Zhang *et al.*, 2015; Brohi *et al.*, 2017). Therefore, a new design for effective nanocarriers that are rigid and controllable has been proposed.

Drug delivery nanosystems are technologies that involve the introduction of therapeutic tools or compounds, such as polymer-drug linkages, liposomes and nanomaterials, to improve treatment safety and efficacy by manipulating the release rate and target release site (Demetzos & Pippa, 2013; Vasir *et al.*, 2005^b). Nanosystem must be more biocompatible than other biomedical devices (Demetzos & Pippa, 2013). Although NPs have been applied in drug delivery nanosystems, their toxicity has encouraged studies on various nanosystems with different nanostructures, such as TNA with and without polymer conjugates. The main objective of drug delivery nanosystems is to increase drug delivery efficacy, stability and specificity with reduced side effects (Dhapte *et al.*, 2019). The optimisation of nanosystem parameters and polymer formulations to construct efficient nanosystems has been widely investigated.

2.2 TNA as a smart drug delivery nanosystem

2.2.1 Fabrication of TNA

The fabrication of TNA was first introduced by Zwilling *et al.*, 1999. TNA with various lengths and diameters (inner and outer) can be produced via electrochemical anodisation (EA) (Kulkarni *et al.*, 2016; Haring *et al.*, 2012; Lai & Sreekantan, 2012). Four generations of TNA have been successfully produced in the past years. The first-generation TNA with a maximum length of 0.5 mm was fabricated in a hydrofluoric solution. The length of the next-generation TNA reached an average of 7 μm in aqueous electrolytes with controllable electrolyte pH levels. The third-generation with lengths of up to 1 mm were fabricated in organic, nonaqueous and polar electrolytes. Finally, fourth-generation TNA was produced in electrolytes without fluoride salt (Radiyan & Raja, 2012).

Numerous reports have discussed the effect of temperature, pH, anodisation period and applied voltage on the dimensions and stability of TNA. In addition, TNA's crystallinity influenced by the uses of different annealing gas such as argon, oxygen and nitrogen gas also apparently affected surface energy and stability (Seo *et al.*, 2014; Liu *et al.*, 2008). In recent years, various applications with TNA have been studied due to the exceptional properties of TNA. TNA has been applied as promising nanomaterials and implants, given their exceptional characteristics, such as antibacterial potential (Jarosz *et al.*, 2015). Aside from the listed uses, the biomedical applications, especially in drug loading and cell adhesion, of TNA with several morphological modifications were studied in the present work.

TNA nanosystems also have excellent capability to interact with cells based on TNA diameter. Wang *et al.*, 2017 stated that TNA with diameters of less than 30 nm could better promote cell adhesion and proliferation than those with more than 100 nm, which also agreed with our work and displayed in Figure 2.3 Cells with good biocompatibility with TNA include human osteoblast cells (Khrunyk *et al.*, 2019; Ueda *et al.*, 2018; Yoon *et al.*, 2014). Therefore, TNA is suitable as biomedical implants. Moreover, the TNA nanostructure is similar to bone morphology and thus promotes cell differentiation, vital for bone remodelling. In a study on blood cell adhesion, Roy *et al.*, 2007, showed that TNA could stop bleeding by stimulating fibrin formation. TNA has attracted considerable attention as a drug delivery system and thus have been explored as nanocarriers for therapeutic delivery, given their unique physical and chemical properties.

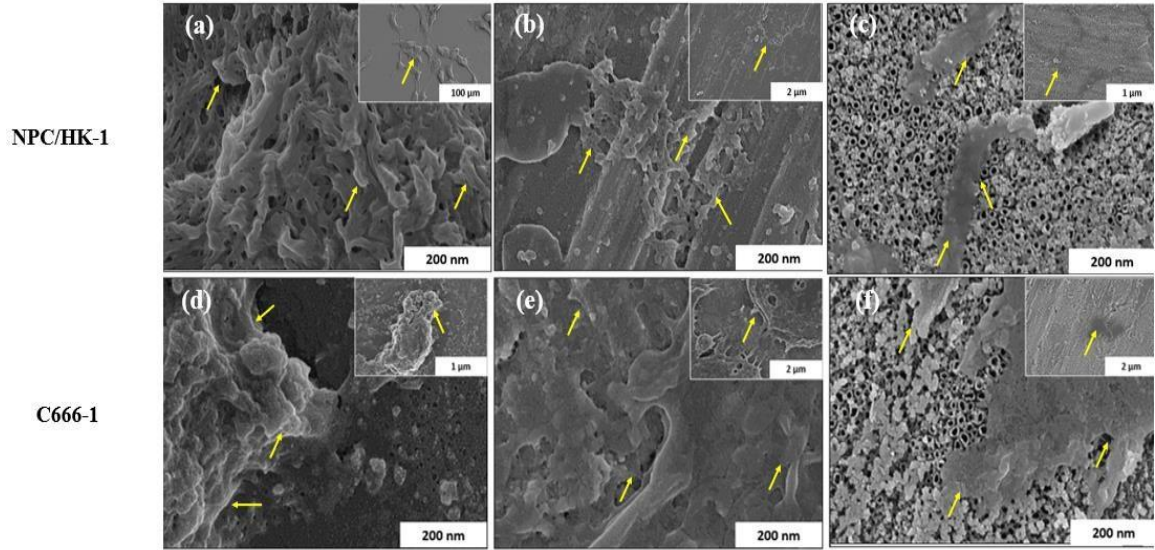


Figure 2.3 The biocompatibility of the NPC cells in terms of cell interaction with the TNA surfaces (average diameter of 60 nm). The elongation of filopodia demonstrated the ability of the surface to promote cell adhesion and proliferation after 48-h incubation.

2.2.2 Physiochemical properties of TNA

One of the critical features of TNA is its nanotube structure, which is favourable for cell attachment because it mimics the structure of bone. TNA can carry numerous biological components, such as proteins, genes and medicinal agents, because of their tube-like nanostructures, which provide a considerable surface area per volume of the structure (Wang *et al.*, 2017). As reported by Kafshgari *et al.*, 2019, the controllable length of TNA slows drug release upon encapsulation due to entrapment during loading. With these exceptional characteristics, TNA can be utilised in smart drug delivery, especially long-term and sustained release. The nanostructures of TNA may be a potential alternative in the delivery of drugs, especially chemodrugs, considering the instability of chemodrugs and the need to minimise burst release upon interaction with the target site.

TNA exhibit the perfect morphology for encapsulating drugs considering their nanotube features. TNA also possess hydrophilic surfaces that can overcome the hydrophobic properties of drugs commonly studied in TNA drug delivery. Therefore, nanomaterials with hydrophilic characteristics may provide an alternative in delivering drugs to target sites at safe doses. In the present work, CDDP with hydrophilic properties was loaded into a TNA nanosystem to promote its efficient delivery to the target site. Furthermore, the prolonged and sustained release CDDP administration may increase the post-treatment effect by regulating the diameter and length of the TNA nanosystem.

2.2.3 TNA potential for targeted cancer therapy

The potential of TNA in drug delivery has already been acknowledged in countless studies (Kunrath *et al.*, 2018; Wang *et al.*, 2017). Notably, besides anti-inflammatory factors, vitamins and genes, chemodrugs have been explored for drug loading into TNA for cancer therapy. TNA is used mainly due to its hydrophilicity and nanotube structures presented in Figure 2.4, which play an essential role in controlling drug release in the studied environment. Some hydrophilic chemodrugs, such as CDDP and doxorubicin (Hong *et al.*, 2012), are also studied together with TNA for controlled drug release activity. These drugs are easier to incorporate into body fluid than hydrophobic ones. The one-open-ended nanotube structure of TNA increases drug loading efficiency and decelerates drug release in the presence or absence of a polymer. The related feature can minimise drug burst release and thus reduce the toxicity induced by high doses of chemodrugs.

2.3 Smart drug delivery involving biopolymer coating technology

Smart drug delivery is used to describe the process wherein drugs are released at a very slow pace or are not released until reaching the site of action. Release occurs at a controllable rate only when the targeted site is reached (Liu *et al.*, 2016). The controllable release can be achieved by adding a biopolymer coating that protects the drug–nanomaterials from degradation or damage before reaching the target site (Gandhi *et al.*, 2012). The main objective of smart drug delivery is to exert the full effect of the administered drug directly on the target site while minimising side effects (Sanadgol & Wackerlig, 2020; Liu *et al.*, 2016). Biopolymer coatings are often used in smart drug delivery technologies to increase the functionality of the drug-loaded nanosystem because of their flexibility, ease of degradability, and lack of toxicity to cells. As a result, these coatings improve drug delivery success rates.

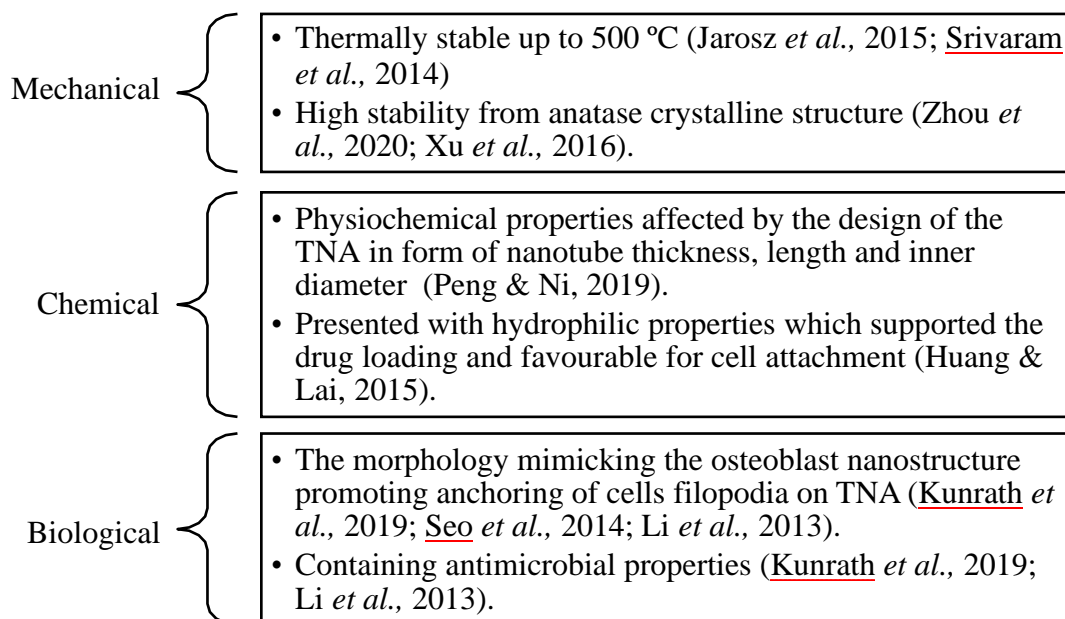


Figure 2.4 Mechanical, chemical and biological properties were befitting the biomedical properties of TNA. The most frequently mentioned characteristics of TNA in the biomedical application were compiled, focusing on the cell interaction, strength and stability of the nanostructures.

2.3.1 Type of biopolymer coating technology

Biopolymers are divided into three groups: polynucleotide, polypeptide- and protein-based and polysaccharide-based biopolymers (Gutierrez *et al.*, 2021; Reddy *et al.*, 2021;). Hybridisation and enzyme reactions are used to synthesise polynucleotide-based polymers, subjected to multiple optimisation processes before transformation into hydrogel scaffolds. Although biopolymers have superior programmability for DNA-related material, the synthesis is tedious thus need careful attention to minimise polymer degradation (Gačanin *et al.*, 2020). Polypeptide- and protein-based polymers are composed of long chains of amino acids from living organisms. The degradation and production of these polymers required enzymatic reactions to break down protein. Despite their excellent stability, these polymers are fragile due to their low mechanical strength. Protein-based polymers are at high risk for rejection by the immune system and lead to an immunogenic response, thus unfit for biomedical implantation (Reddy *et al.*, 2021).

Due to their relevance, polysaccharide polymers are frequently studied and applied in the biomedical field. The benefit of polymers, including antimicrobial activity, good biocompatibility, and degradability, was applied in the study for colon bacteria (Umadevi *et al.*, 2010); high tensile strength (Avcu *et al.*, 2019) and anti-cancer effect (Abedian *et al.*, 2019). Chitosan, which is synthesised through the derivation of the partial deacetylation of chitin, a by-product of the shellfish (coral, crab and shrimp) exoskeleton, as well as mushroom and fungi (Abedian *et al.*, 2019), best fits these characteristics. The use of chitosan in wound healing, drug delivery, and tissue engineering has been studied due to chitosan's special interlinkage with growth factors and the extracellular matrix (Reddy *et al.*, 2021).

Chitosan has shown positive outcomes in specific drug delivery, especially smart drug delivery. The application of chitosan in drug delivery has been comprehensively reviewed by Parhi, 2020, who covered several topics, including oral, buccal, periodontal transdermal and topical drug delivery. Generally, chitosan promotes improved drug delivery towards the target site while preventing burst release to minimise toxicity (Jia *et al.*, 2015). In treating tuberculosis, rifampicin NPs were used together with chitosan and successfully maintained sustained release for 24-h without toxicity in the *in vitro* stage (Rawal *et al.*, 2017). Despite its favourable benefits in drug delivery, chitosan coating has several limitations: low solubility, poor mechanical strength, and high swelling capability (Parhi, 2020). Various works involving chitosan have been conducted with multiple optimisation processes to improve the properties of chitosan in smart drug delivery technology, as listed in Table 2.2.

Table 2.2 Parameters importance in the preparation of chitosan for biopolymer coating. The parameters are vital for the biocompatibility and functionality of chitosan in biomedical applications.

Reference	Amount of chitosan	Diluent	Method of coating	Number of coating (s)/ Thickness of coating	Application
Rahnamaee et al., 2021	2 % (w/v)	dH ₂ O	Drop casting of 10 µL of chitosan liquid	No information	The addition of chitosan is effective for prolonging antibacterial activities and promoting the viability of bone cell
Hashemi et al., 2020	2.5 % (w/v)	0.8 % (v/v) acetic acid	Spin coating at 1000 rpm, 60 sec	15 layers	Sustained release of chitosan-coated TNA-loaded Metformin for mesenchymal stem cell growth activities
Vakili & Asefnejad, 2020	0.5 % (w/v)	0.5 % (v/v) Acid solution	Spin coating at 1000, 4000, and 8000 rpm for 30 sec	Three times	Observation on the antibacterial properties of both TNA and chitosan-coated surfaces to improve bone regeneration and biocompatibility
Pawlik et al., 2019	0.25 % (w/v)	1 % (v/v) acetic acid, ethanol and dh ₂ O	Electrophoretic disposition (EPD)	No information	To study the effect of chitosan coating by EPD method on TNA surface by mechanical and surface properties
Mokhtari et al., 2018	1 % (w/v)	2 % (v/v) acetic acid	Dip coating	Three times	Improvement on TNA substrate bioactivity through MG63 cell attachment and proliferation
Shidfar et al., 2017	1 % (w/v)	0.8 % (v/v) acetic acid	Dip coating	One dip-drying (thin coating), three dip-drying (thick coating)	Preventing the initial release of the drug and antimicrobial properties for orthopaedic and dental implant application

Feng <i>et al.</i>, 2016	1 % (w/v)	0.8 v/v % acetic acid	Top-filling	A total of 10 μ L chitosan liquid was dropped on the TNA-loaded drug surface	Preventing bacterial infection from the process of orthopaedic implant
Kumeria <i>et al.</i>, 2015	1 % (w/v)	0.8 % (v/v) acetic acid	Dip-coating	Approximately 1.5 μ m	Antimicrobial, stimulator for the growth of the osteoblast cell, and TNA-based implant protective layer
Gulati <i>et al.</i>, 2012	1 % (w/v)	0.8 % (v/v) acetic acid	Dip coating	One to five layers	The chitosan coating allows for drug distribution with predictable kinetics and a longer time.

2.3.2 Parameter in drug controlled released strategies

Other researchers have found that chitosan performs excellently in slowing drug release activity due to several factors, such as diluent concentration in chitosan preparation, chitosan thickness and coating method. Acetic acid is the most frequently used acid (Kou *et al.*, 2020) in the dissolution of chitosan due to the poor solubility of chitosan in water. Other weak acids such as propionic and formic acid were also previously used for chitosan preparation (Li *et al.*, 2006), resulting in a higher degree of deacetylation (DD). Mohan *et al.*, 2016, reported that a higher concentration of acetic acid (2%) degrades chitosan coating faster than a lower concentration of acetic acid (1%) and thus accelerates drug release. This phenomenon can be attributed to the increase in protonation degree due to weak chitosan interaction at high concentrations of acetic acids (Rinaudo *et al.*, 1999). This condition primes the hydrogen in chitosan to interact with water and, therefore, increases chitosan's solubility in the immersion buffer.

The thickness of the chitosan coating also influences the rate of drug delivery. Mohan *et al.*, 2016, determined chitosan thickness using atomic force microscopy, and Hashemi *et al.*, 2020, described thickness based on coating layer number. Both works agreed on the importance of chitosan coating thickness in slowing drug release. Furthermore, Abedian *et al.*, 2019, considered the biocompatibility of chitosan in a study on the effects of the various molecular weights of chitosan on various cells. They found that the anti-cancer effect of chitosan is not affected by molecular weight and that cancer cell death is caused by necrosis.

In contrast, Wimardani *et al.* (2012) found that the toxicity of chitosan was heavily influenced by the molecular weight of the compounds, with high molecular weight chitosan being a better promoter for cell function than low molecular weight chitosan. The chitosan cytotoxicity for *in vitro* and *in vivo* may also be negligible as long the administration dose was strictly monitored. The safety and the functionality of chitosan had been widely proven, as presented by Shivakumar *et al.*, 2021 in their paper regarding the patent administered for chitosan under the biomedical application. The toxicity of chitosan must be investigated to develop the best chitosan-coated nanosystem for smart drug delivery.

2.4 Prospects: Targeted chemodrug treatment for NPC

This nanotechnology has attracted worldwide attention due to its functionality and potential in preclinical works (Kim & Khang, 2020; Patra *et al.*, 2018), as listed in Figure 2.5. Currently, the available and approved cancer treatment is brachytherapy. This radiation therapy is provided in capsules, seeds or ribbons containing a radiation source and placed specifically at tumour sites or surroundings (NIH, 2019). A study on brachytherapy for pancreatic cancer found that the presence of chemodrugs after irradiation from brachytherapy is essential for achieving good results (Luo *et al.*, 2021). In agreement with the previous work, Murakami *et al.* (2020) also supported the application of brachytherapy as a new option for NPC treatment, as illustrated in Figure 2.6. The potential of nanomedicine for drug delivery through a chitosan-coated TNA nanosystem loaded with chemodrugs may have promising outcomes in the related application of brachytherapy in NPC cancer treatment.

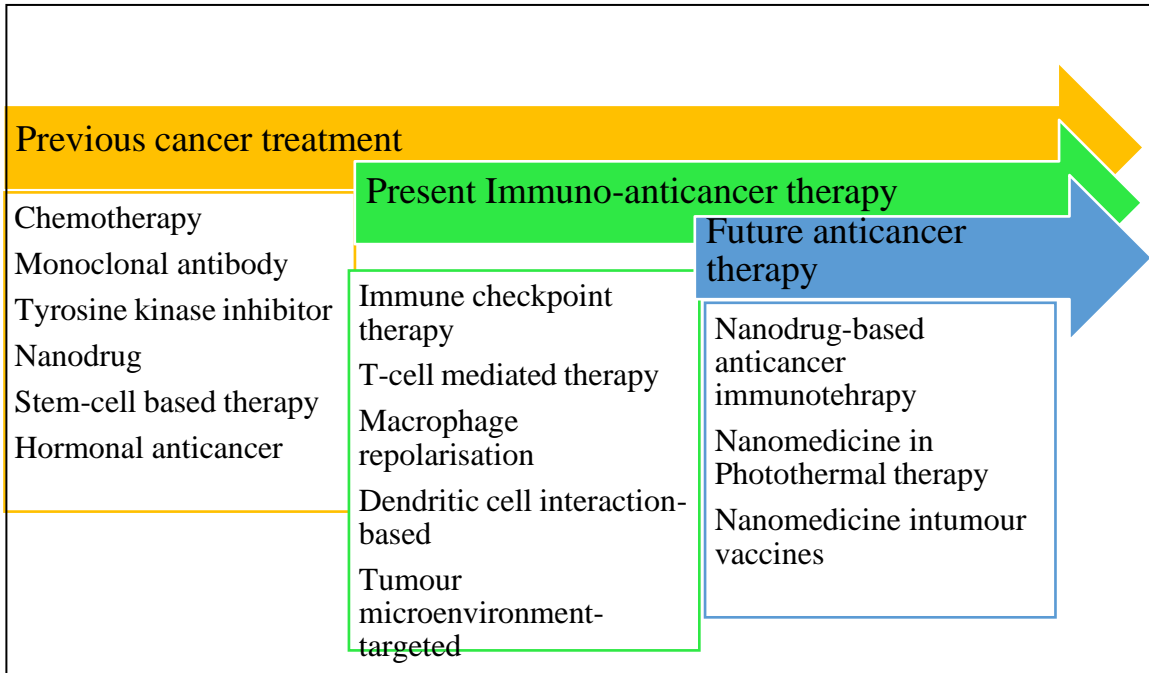


Figure 2.5 The research on cancer treatment in the past, existing, and future has been simplified according to Kim & Khang, 2020. Cancer location was the aim of past treatment; meanwhile, existing cancer therapy focused on the microenvironment of carcinoma. Future research on the utilisation of nanomedicine technology might be applied in drug distributions by manipulating nanosized materials.

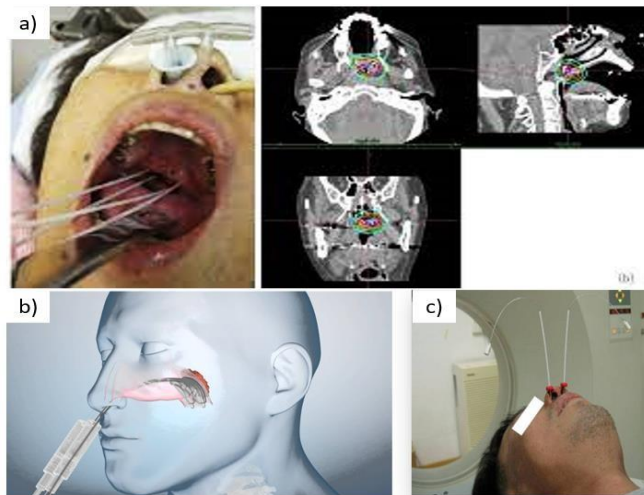


Figure 2.6 HDR-ISBT treatment in a patient with stage T3 NPC. Image (a) illustrated the brachytherapy application via an inserted needle adapted from Murakami *et al.*, 2020, (b) displayed the 2D image of brachytherapy prototype and (c) showed the example of patient with the device.

CHAPTER 3

METHODOLOGY

3.1 Introduction

This chapter consists of four sections. The first section elaborates on the raw materials, chemicals, and solvents used throughout the experimental work. The second section explained the experimental design of this work and described the parameters studied. The third section outlines the experimental procedure for TNA anodisation, optimisation of CDDP loading, and biphasic release activities in phosphate buffer saline (PBS). Subsequently, CDDP quantitative techniques and characterisations for chitosan-coated CDDP-TNA were performed to identify and confirm CDDP loading. ICP-OES of chitosan-coated CDDP-TNA further characterised detection of CDDP in simulated body fluid (SBF). The fourth section of this paper explores the functional aspects of the chitosan-coated CDDP-TNA nanosystem in an *in vitro* model.

3.2 Raw materials and chemicals

The raw materials and chemicals used in this work are summarised in Table 3.1. All the materials are commercial products and were utilised without additional purification or treatment otherwise specified in the methods described. All plasticware and glassware such as microcentrifuge tubes and pipette tips were sterilised by autoclaving at 121 °C for 20 mins before experiments. Before autoclaving, TNA samples were cleaned with 70 % (v/v) ethanol and rinsed with deionised H₂O. All the materials were dried in a drying oven overnight. The solutions or buffers were sterilised before each experiment by either filtering using a 0.02-micron filter system or using an autoclave